Journal of Alloys and Compounds 509 (2011) 3576–3581

Contents lists available at ScienceDirect

Journal of Alloys and Compounds

journal homepage: www.elsevier.com/locate/jallcom

Shape-controlled synthesis and photocatalytic properties of three-dimensional and porous zinc oxide

Peiyan Ma[a,b,*], Yan Wu[b], Zhengyi Fu[a], Weimin Wang[a]

[a] State Key Laboratory of Advanced Technology for Materials Synthesis and Processing, Wuhan University of Technology, Luoshi Road, Wuhan 430070, PR China
[b] School of Science, Wuhan University of Technology, Wuhan 430070, PR China

ARTICLE INFO

Article history:
Received 28 June 2010
Received in revised form
10 December 2010
Accepted 10 December 2010
Available online 21 December 2010

Keywords:
Porous zinc oxide
Citrate–ZnO interaction
Specific surface area
Photocatalytic activity

ABSTRACT

In this study, we reported a method for growing macroporous ZnO on a large scale via a facile solution-based method using citrate as crystal growth modifier. The microstructures were studied by X-ray diffraction, scanning electron microscopy, FT-IR, UV–visible spectrometer and N_2-physisorption techniques. Influencing factors on the morphology of ZnO were discussed, including anion species of Zn^{2+} precursor, adding sequence of sodium citrate, sodium citrate concentration and reaction time. On the basis of the investigation on the growth process, citrate ion–ZnO interaction was vital to the formation of complex structure, which was accompanied by acetate ion induction to form the high-quality macroporous spheres. UV–Vis results exhibited a blue-shift when compared with conventional-sized zinc oxide. The large specific surface area of porous ZnO resulted in enhanced absorption of Rhodamine B and improved photocatalytic activity.

1. Introduction

In recent years, porous transition metal oxides with pore size ranging from 2 to 200 nm are of technological interest as photocatalysts and sensor materials [1]. These kinds of metal oxides could attach the remarkable photocatalytic properties of conventional porous materials to advanced metal oxide. Porous metal oxide has a large surface area because of its confined porous structure and high surface to volume ratio. As a result, it should behave high photochemical activity because of the improved interaction between catalyst and guest organic molecules [2,3].

ZnO is one of the most widely studied semiconductors for use in solar cells, sensors, ultraviolet nanolasers and light-emitting diodes (LEDs) [4]. The electronic and optical properties of ZnO nanostructures are largely dependent on their composition and crystal structure. Synthesis of nano zinc oxide in aqueous solution has the advantages of simplicity, low cost, lower reaction temperature and large scale production. The surface modification of ZnO can also be carried out. The crystal morphology of nano material is determined by the crystal structure of the initial crystal seed and the interaction of different crystal seed facets with capping agents [5]. Different template molecules, such as polymers [6,7], capping agents [8], biomolecules [9] and coordination agents have been adopted to fabricate morphologically and functionally distinct ZnO nanostructures. The binding affinity of template molecule can vary from one crystal facet to another, which would exert preferential effect and effectively hinder the growth of a certain crystal facet, thus provides a means for synthesis of zinc oxide with special functions. The synthesis of porous zinc oxide has been rarely reported, because the porous structure is easy to deform and collapse under high temperature conditions due to its thermodynamic instability [10]. So far, the development of economical methods suitable for the large-scale synthesis of ZnO porous structures with high catalytic activity and easy separation signifies a critical challenge to their practical applications.

Sodium citrate, in particular, is an effective capping agent capable of blocking surfaces from chemical reactivity. Citrate anions [11] would preferably bind on the specific facet of ZnO crystal to prohibit the nucleation and crystal growth along the orientation, which is similar to the inhibition characteristics induced by ascorbic acid [12] and polyacrylamide [13].

In this paper, we reported a synthesis method of a macroporous crystal structure of ZnO under mild conditions. ZnO macroporous structure with uniformly sized hexagons was found to be built from stacking of nanoplates. We employed sodium citrate, which had a strong ability to coordinate with transition metal ions, as structure-directing agent for the polar surfaces of ZnO. A variety of advanced testing technologies were used to describe the formation mechanism of these porous ZnO. This study is believed to be a reference for other macroporous transition metal oxides.

* Corresponding author. Tel.: +86 27 87865484; fax: +86 27 87215421.
E-mail address: mapeiyan0833@tom.com (P. Ma).

0925-8388/$ – see front matter © 2011 Elsevier B.V. All rights reserved.
doi:10.1016/j.jallcom.2010.12.073

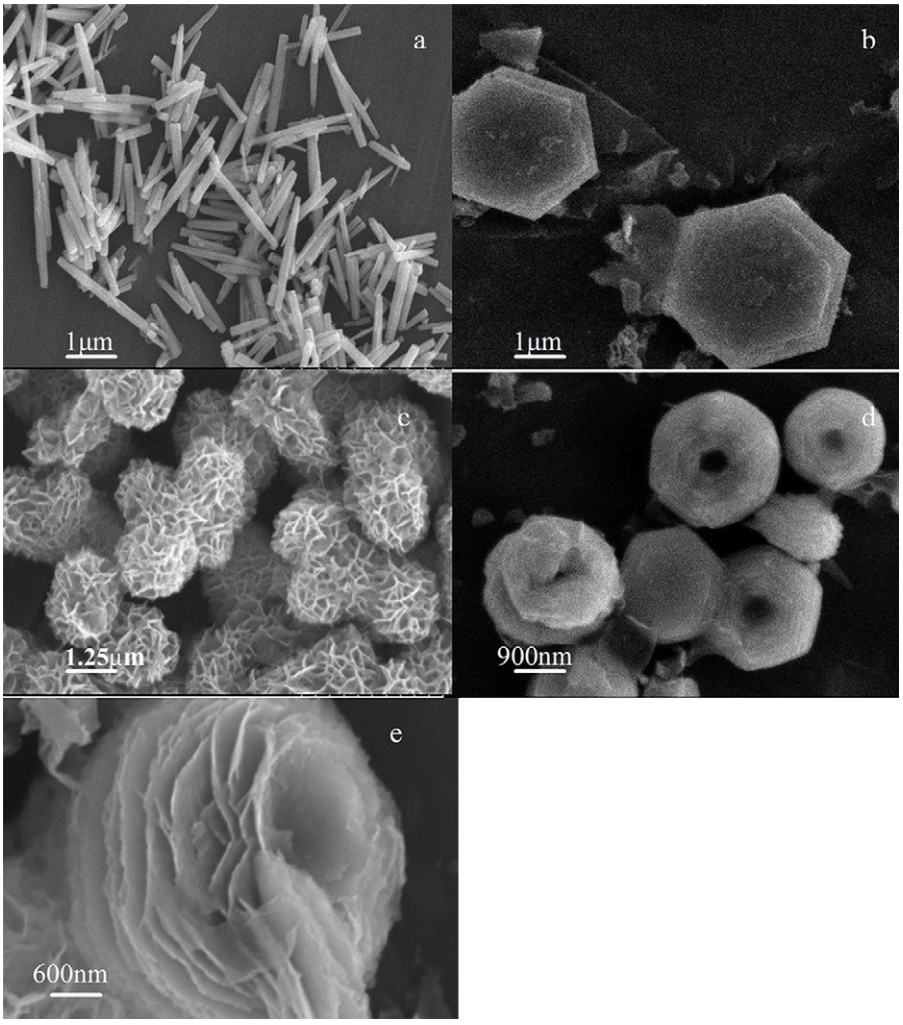

Fig. 1. SEM images of (a) primary ZnO rods, (b) ZnO lamellar structure, (c) porous ZnO spheres, (d) ZnO stacking nanoplates and (e) ZnO stacking nanoplates treated with sonication.

2. Experimental

2.1. Materials

Zinc acetate dihydrate, zinc nitrate hexahydrate, hexamine and sodium citrate were obtained from China National Pharmaceutical Industry Corporation Ltd. All chemicals used in this work were of analytical grade and were used without further purification.

2.2. Characterization

The morphologies of the as-synthesized samples were observed using JSM-5610LV Scanning Electron Microscope. The phase structures of the samples were identified by Rigaku ultimaIII diffractometer power X-ray diffraction. FT-IR spectra were measured with a Nexus Fourier transform infrared spectrophotometer (Thermo Nicolet, America). The UV–visible absorption was measured on Shimadzu UV-2550 spectrometer with pure $BaSO_4$ as the reference. N_2 adsorption–desorption isotherms were collected on an ASAP 2020 (Micrometrics) surface area analyzer at −196 °C. Before the measurements, the samples were outgassed at 260 °C in a vacuum for 6 h. The BET method was used to calculate the specific surface areas using desorption data.

2.3. Synthesis

In a typical synthesis, the aqueous solution containing zinc acetate dihydrate (0.02 M), hexamine (0.02 M) and sodium citrate (3.4×10^{-4} M) was prepared with 350 mL deionized water. After magnetic stirring for 1 h, the reaction mixture was transferred to 90 °C water bath. After 6 h, the white precipitation was gained by centrifuging, washed with distilled water and absolute ethanol several times and finally dried at 60 °C for 12 h. The obtained samples were heated to 600 °C to remove the organics. To study the role of sodium citrate, the reaction was carried out in the absence and presence of different concentrations of the capping agent under same reaction conditions. Factors of the type of zinc salt, reaction time and the adding sequence of sodium citrate were also considered.

2.4. Photocatalytic activity measurements

The photocatalytic activity was investigated using RhB aqueous solution as a probe and a petri dish as the photoreactor vessel. The reaction system containing 100 mL of RhB solution with an initial concentration of 2.5×10^{-5} M and 30 mg of ZnO (ZnO rods or porous ZnO) was magnetically stirred in the dark for 0.5 h to reach adsorption equilibrium. The solution was then exposed to UV irradiation from a 200 W high-pressure Hg lamp (the strongest emission at 365 nm) at room temperature. The supernatant was collected every 10 min to measure the RhB degradation by UV vis spectra.

3. Results and discussion

3.1. Structural properties

Fig. 1a shows the SEM photograph of the primary ZnO rods prepared with $Zn(NO_3)_2$ and hexamine for 6 h. It can be seen that these rods have well-defined hexagonal crystallographic planes, about 250 nm in diameter and 1–2 μm in height. ZnO crystal lattice is described as alternating planes composed of Zn^{2+} and O^{2-} which are stacked alternatively along the crystallographic *c*-axis. ZnO tends to grow along the *c* axis to form rod-like microparticles for the specific crystalline structure [14].

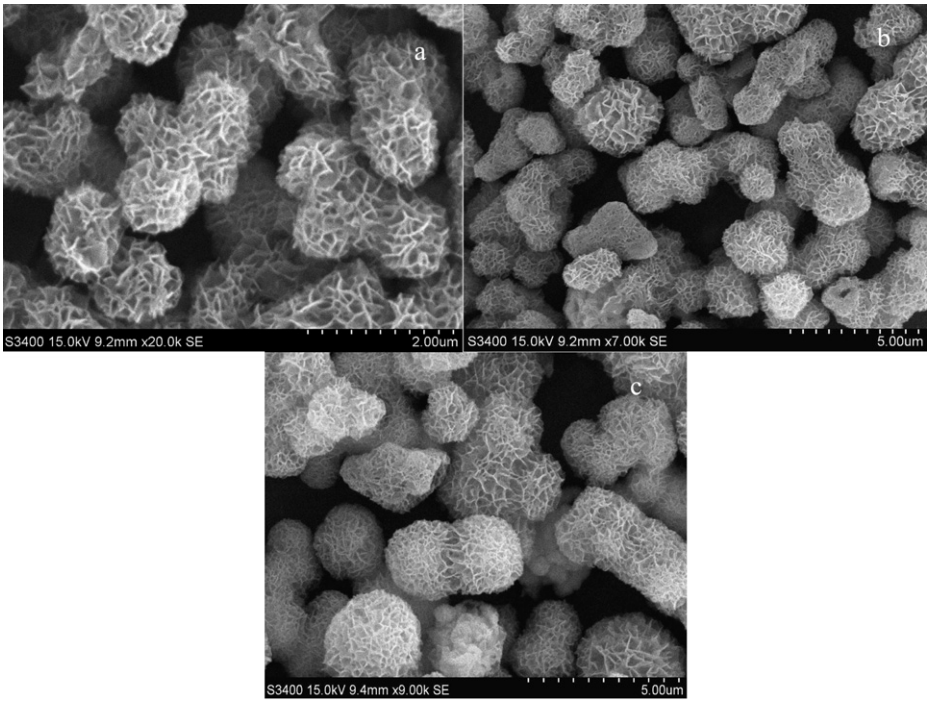

Fig. 2. Scanning electron microscopic images of the citrate concentration series samples treated for 6 h. (a) 3.4×10^{-4} M, (b) 8.5×10^{-4} M and (c) 1.27×10^{-3}M.

If 3.4×10^{-4} mol L^{-1} sodium citrate was added to $Zn(NO_3)_2$ and hexamine solution, under the same temperature and reaction time, hexagonal lamellar structure of zinc oxide was obtained, as shown in Fig. 1b. As reported in the literature [15,16], citrate was a biological ligand which could form complexes with Zn^{2+}. It plays an important role in the formation of lamellar structures by bonding to the Zn^{2+} (0 0 0 1) surfaces through the $-COO^-$ and OH^- [17]. The crystal growth along the (0 0 1) orientation was suppressed, which led to crystal growth along sideways and the formation of platelike nanostructures. Liu [18] obtained similar lamellar structure with PEG as the stabilizer.

When zinc nitrate was replaced by zinc acetate in the solution containing the same concentration of sodium citrate and hexamine, porous zinc oxide spheres with diameter of 2.5 μm were formed, indicated that the impact of acetate ion on the formation of porous structure. Observed from Fig. 1c, the large porous spheres were composed of well-defined primary lamella of tens of nanometers in thickness. The macropores, similar to the deformation of the honeycomb hexagon, are closely connected together to form three-dimensional network. In the forming process of lamellar ZnO, Zn^{2+} not only coordinated with citrate, but also interacted with CH_3COO^- through strong electrostatic attraction. OH–, which released from the hexamine, had stronger binding ability to replace CH_3COO^- groups and developed new ZnO lamella. So the secondary nucleation resulted in the formation of porous structure [19].

The adding sequence of sodium citrate was also crucial. When sodium citrate was mixed thoroughly with zinc acetate before adding of hexamine, ZnO stacking nanoplates with a diameter of 2 μm were produced. Microstructure in Fig. 1d also shows there is a hexagonal hole in the middle of ZnO nanoplate. After the growth of ZnO crystal reaching certain equilibrium, the dissolution effect became more dominant. Since the polar plane (0 0 0 1) of ZnO had the higher surface energy, the dissolution rate of the polar plane (0 0 0 1) was faster than that of the nonpolar plane (1 0 1 0). The CH_3COO–, which adsorbed on the lateral surfaces, slowed down the dissolving velocity of the lateral surfaces. So the selective dissolution of ZnO resulted in the formation of the hexagonal hole [20,21]. Rizia suggested that the observed morphology might be due to the simultaneous occurrence of Ostwald ripening and oriented attachment during the growth of crystals [22].

The loose lamellar structure of ZnO shown in Fig. 1e indicates the existence of van der Waals forces [23]. Van der Waals force originates from molecular deformability of zinc oxide, which could be explained by zinc ion polarization force and deformation of oxygen ions.

The influence of sodium citrate concentration on the morphology was discussed to better understand the formation mechanism of porous structure. The sodium citrate concentrations were set to 3.4×10^{-4}, 8.5×10^{-4}, 1.27×10^{-3} and other conditions remained unchanged. Seen from Fig. 2a–c, all of the morphologies are shown as porous zinc oxide microspheres structure. As the sodium citrate concentration increased, the average pore size gradually increased from 100 nm to 300 nm with little change in wall thickness. Meanwhile, the adhesion contact between the spheres led to the formation of irregular shape.

Following the foregoing discussion, porous zinc oxide spheres structure was the synergy effect between citrate ion and acetate ion. Citrate ion–ZnO interaction was vital to the formation of complex structure, which was accompanied by acetate ion induction to form the high-quality macroporous spheres.

The entire growth process of the macroporous spheres synthesized with a citrate concentration of 3.4×10^{-4} was explored by morphology observation of time series samples as shown in SEM images of Fig. 3. After reaction for 10 min (Fig. 3a), porous microspheres with about 1 μm in diameter had already been formed. From 10 min to 6 h, the diameter of the porous microspheres gradually increased. After 6 h, the diameter was about 2.5 μm, and the growth almost stopped (Fig. 1c). A conclusion was drawn that the porous structure had been formed in the early stage of ZnO, instead of being piled up by ZnO lamella during the subsequent crystal growth process.

After 2.5 h, some layered structure of ZnO appeared, as shown in Fig. 3e and f. It could be clearly seen that the layered structure

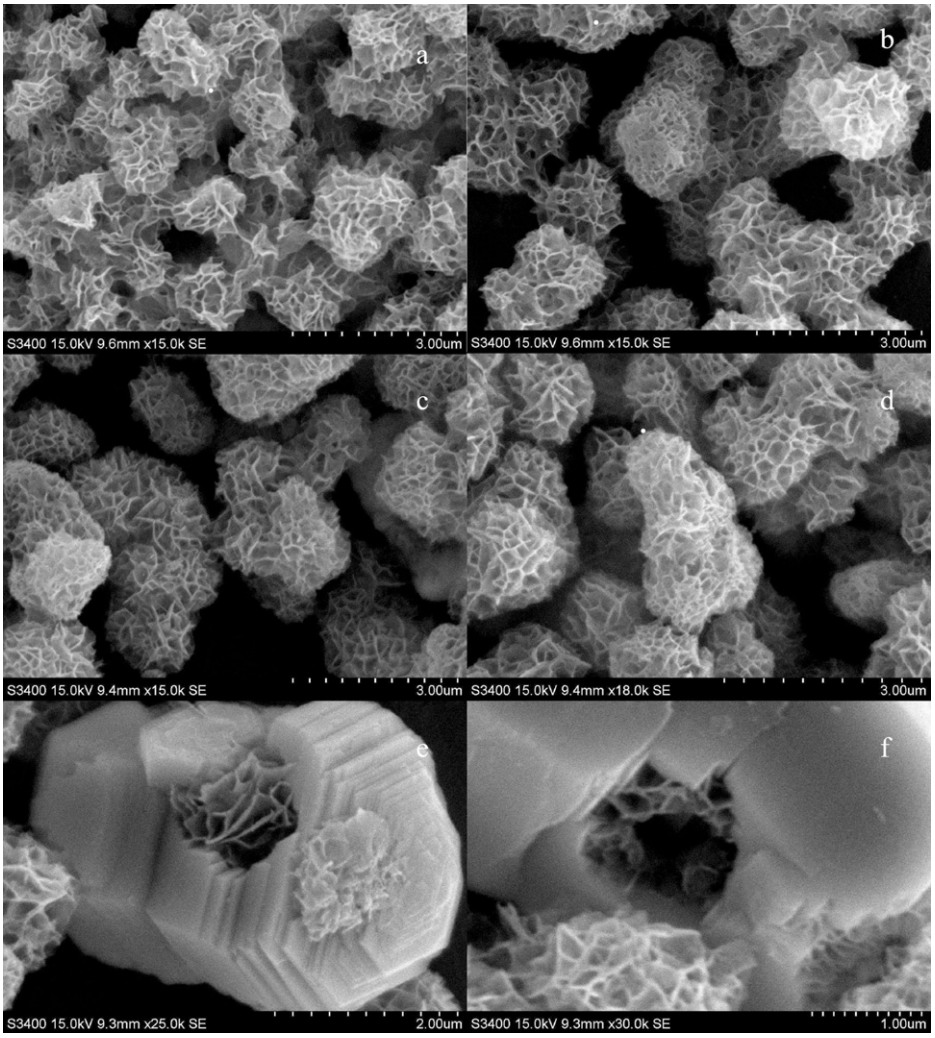

Fig. 3. SEM images of the time series samples treated with citrate concentration of 3.4×10^{-4} (a) 10 min, (b) 0.5 h, (c) 1.5 h, (d) 2.5 h, (e) and (f) some samples appeared after 2.5 h.

had been formed after the deformation of porous zinc oxide. Consequently, porous zinc oxide exhibited thermodynamic instability. If provided sufficient time, porous zinc oxide would be converted to stable layer structure.

Amplified SEM images of Fig. 4 with 3.4×10^{-4} sodium citrate for 6 h further illustrated that the three-dimensional ZnO was irregular honeycomb structure. In other words, porous zinc oxide might have large surface area.

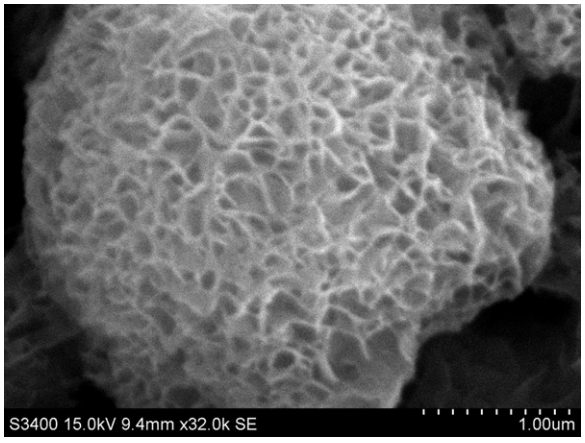

Fig. 4. Amplified SEM images of porous ZnO with 3.4×10^{-4} sodium citrate for 6 h.

The phase structure of the as-synthesized samples was characterized using X-ray diffraction (XRD). Comparative study between the nano rods and porous micro spheres was designed to reveal the growth mechanism of porous microspheres. The sharp diffraction peaks in Fig. 5 indicates the excellent crystalline nature of two samples. The diffraction peaks in the pattern a and pattern b could be assigned to hexagonal ZnO, which were in good agreement with that of the standard card of JCPDS 36-1451. It was obvious that the ratios of relative XRD intensities of (1 0 0)/(0 0 2) were remarkably different between Fig. 5a and b, correspondingly to the rods and porous structures. Similar results had been reported in the literature citations and were attributed to different degrees of growth in preferred orientation [24].

3.2. Fourier transform infrared spectroscopy

To reveal the coordination between sodium citrate and ZnO, ZnO rods and porous ZnO spheres without heat treatment were examined using Fourier transform infrared (FTIR) spectroscopy.

In Fig. 6a and b, the absorption band near 3400 cm^{-1} represented O–H stretching of surface adsorbed water molecule. Adsorption of CO_2 on the metallic cation at 2350 cm^{-1} was clearly examined. The peaks of C–H mode at 2900 cm^{-1} were very weak. In Fig. 6b,

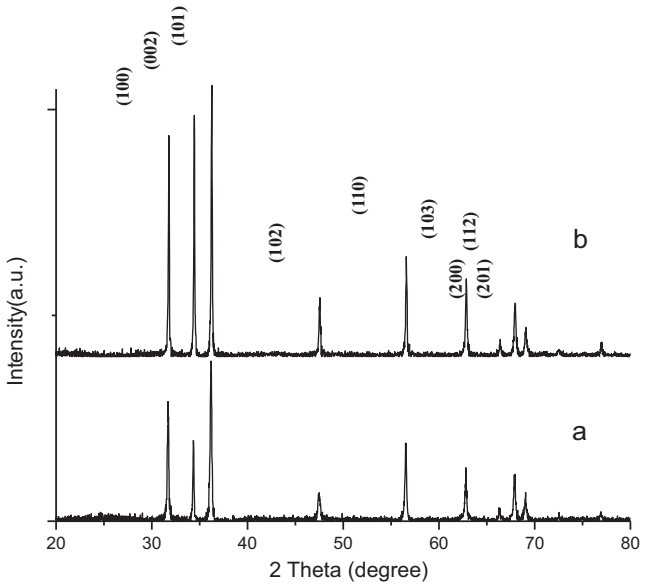

Fig. 5. XRD patterns of the obtained ZnO grown for 6 h in the absence (a) and presence (b) of 3.4×10^{-4} M sodium citrate.

the symmetric and asymmetric stretching bands of COO^- could be examined at 1360 and 1600 cm^{-1}, which did not appear in Fig. 6a. It meant that COO^- of citrate had been combined with zinc oxide. The absorption band at 547 cm^{-1} was referred to stretching mode of ZnO [25] and the reason for the intensity difference between the two spectra was probably because citrate on the surface of ZnO formed a relatively close-packed layer and the molecular motion was inhibited [26]. These data indicated strong coordination ability between Zn^{2+} and COO^-.

3.3. UV–vis absorption spectra

UV–vis absorption was recorded for the investigation on optical properties of the as-prepared products, as shown in Fig. 7. ZnO porous spheres showed the superior performance of UV absorption. The UV–vis absorption peaks centered at 357 nm (Fig. 7a) and 365 nm (Fig. 7b) exhibited blue-shift compared with bulk ZnO (373 nm). Since the diameter of the ZnO nano rods and ZnO porous spheres was larger than the exciton Bohr radius of ZnO, the quantum confinement effect was not considered as the main reason

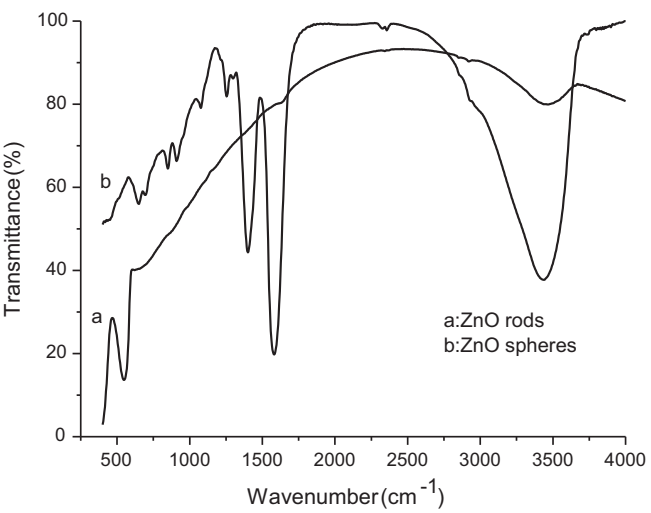

Fig. 7. UV–vis absorption spectra of ZnO rods and ZnO porous microspheres grown for 6 h in the absence and presence of 3.4×10^{-4} sodium citrate.

of the blue-shift. The shift could be correlated with the different scattering of the nano ZnO rods and ZnO porous spheres.

To provide further insight into the inner structure of the hexagonal ZnO architectures, Brunauer–Emmett–Teller (BET) gas adsorptometry measurements were conducted to examine the porous nature of the ZnO hexagonal architectures prepared with citrate concentration of 3.4×10^{-4} for 6 h. The BET specific surface area of the sample was calculated from N_2 isotherms at $-196\,^{\circ}C$, and was found to be as much as about 72.9 m^2/g, which was higher than that of nano rods(0.2491 m^2/g) .The large specific surface area possessed by the sample was mainly due to the existence macropores embedded in the micro architectures.

3.4. Photocatalytic activity

ZnO has been widely used as semiconductor photocatalyst for the photocatalytic degradation of organic pollutants in aqueous solution. Fig. 8 shows the time-dependent absorbance spectrum of the aqueous solution of RhB with ZnO photocatalyst (porous ZnO with 3.4×10^{-4} sodium citrate) and exposure to ultraviolet light for various durations. It could be seen that absorption peaks at 553 nm decreased rapidly with extension of the exposure time,

Fig. 6. FTIR spectra of ZnO rods and porous ZnO with 3.4×10^{-4} sodium citrate.

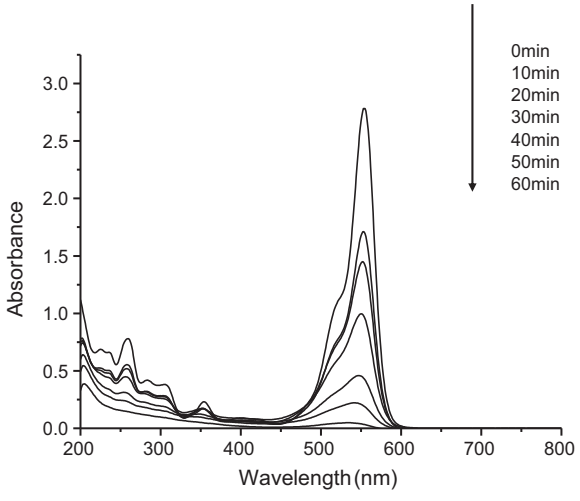

Fig. 8. Time-dependent absorbance spectrum of the RhB solution in the presence of porous ZnO with 3.4×10^{-4} sodium citrate.

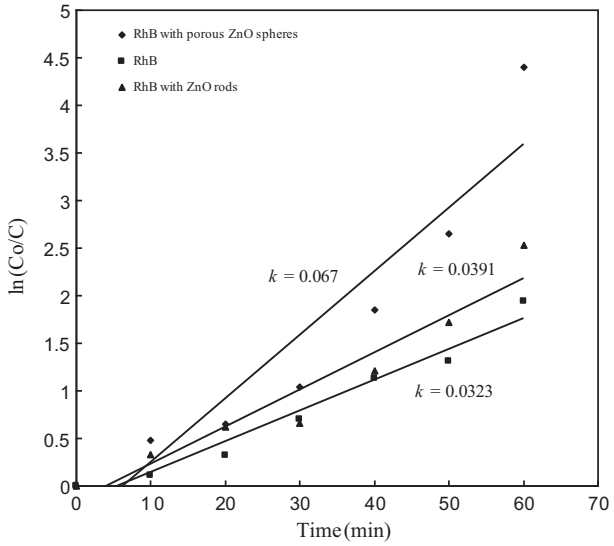

Fig. 9. The $\ln(C_0/C)$ versus time curves of photodegradation of RhB with and without photocatalysts. The experimental data are fitted using the pseudofirst-order kinetic equation: $\ln(C_0/C) = kt$.

and completely disappeared after 60 min.

The photodegradation of RhB can be considered as a pseudo-first-order reaction [27,28], and its kinetics can be expressed as follows:

$$\ln\left(\frac{C}{C_0}\right) = -kt$$

where C_0 is the initial concentration and C is the concentration after the RhB degradation for time t. Fig. 9 shows the photodegradation curves of RhB in the form of $\ln(C/C_0)$ as a function of time. The reaction rate constant k was calculated to be 0.0323, 0.0391 and 0.067 min^{-1} for the RhB without photocatalysts, RhB with ZnO rods, and RhB with porous ZnO spheres, respectively. Without any catalyst, only slow decrease in the concentration of RhB was detected under UV irradiation. The addition of ZnO porous spheres led to obvious degradation of RhB. ZnO porous spheres has not only a large surface area but also a special porous structure, facilitating the increase in adsorption capacity. The assembly structure of ZnO nano lamella enables the efficient charge separation through interparticle charge transfer [29].

4. Conclusions

In summary, we observed a solution-phase reaction for growing porous ZnO using citrate as crystal growth modifiers. The impact of anion species of Zn^{2+} precursor, adding sequence of sodium citrate, concentration of sodium citrate and reaction time on the ZnO structures was discussed. On the basis of the results, we proposed that porous zinc oxide spheres were the synergic effect between citrate ion and acetate ion. The large specific surface area of porous ZnO resulted in enhanced absorption of Rhodamine B and improved photocatalytic activity.

Acknowledgments

We acknowledge National Natural Science Foundation of China (A3 Foresight Program-50821140308) and self-determined and innovative research funds of WUT (2010-1a-042) for support.

References

[1] M.Y. Guo, M.K. Fung, F. Fang, J. Alloys Compd. 509 (2011) 1328–1332.
[2] S.L. Wang, X. Jia, P. Jiang, J. Alloys Compd. 502 (2010) 118–122.
[3] Y. Huang, Z. Ai, W. Ho, J. Phys. Chem. C 114 (2010) 6342–6349.
[4] Y Fahrettin, J. Alloys Compd. 494 (2010) 451–455.
[5] M. Matin Sadat, L. Aidin, A. Simchi, J. Alloys Compd. 485 (2009) 616–620.
[6] X. Shi, L. Pan, S. Chen, Langmuir 25 (2009) 5940–5948.
[7] Z. Zhang, X. Li, C. Wang, J. Phys. Chem. C 113 (2009) 19397–19403.
[8] L. Wang, G. Liu, L. Zou, Nano Lett. 493 (2010) 471–475.
[9] H. Liu, B. Huang, Z. Wang, J. Alloys Compd. 507 (2010) 326–330.
[10] J. Zhang, S. Wang, M. Xu, Cryst. Growth Des. 9 (2009) 3532–3537.
[11] S. Li, L. Ge, H. Gu, J. Alloys Compd. 509 (2011) 94–98.
[12] Y.C. Chang, W.C. Yang, C.M. Chang, Cryst. Growth Des. 9 (2009) 3161–3167.
[13] S. Cho, J.-W. Jang, J.S. Lee, Langmuir 26 (2010) 14255–14262.
[14] Y. Tao, M. Fu, A. Zhao, J. Alloys Compd. (2010) 99–102.
[15] S. Cho, J.-W. Jang, S.-H. Jung, Langmuir 25 (2009) 3825–3831.
[16] R.T. Zhengrong, A. James, J.L. Voigt, J. Am. Chem. Soc. 124 (2002) 12954–12955.
[17] J. Liang, J. Liu, Q. Xie, J. Phys. Chem. B 109 (2005) 9463–9467.
[18] X. Liu, M. Afzaal, R. Karthik, J. Am. Chem. Soc. 131 (2009) 15106–15107.
[19] D. Zhang, L. Sun, J. Zhang, Cryst. Growth Des. 8 (2008) 3609–3615.
[20] Q. Yu, W. Fu, C. Yu, J. Phys. Chem. C 111 (2007) 17521–17526.
[21] H. Guo, Z. Lin, Z. Feng, J. Phys. Chem. C 113 (2009) 12546–12550.
[22] B. Rizia, H. Wang, T. Felicia, Langmuir 23 (2007) 5843–5847.
[23] F. Li, Y. Ding, P. Gao, Angew. Chem. 116 (2004) 5350–5354.
[24] S.K. Park, Y.K. Lee, H.T. Kwak, J. Phys. Chem. C 112 (2008) 4129–4133.
[25] D. Jaykrushna, K. Deepa, J. Phys. Chem. C 114 (2010) 2544–2550.
[26] S.-G. Kim, W.-N Wang, T. Iwaki, Phys. Chem. C 111 (2007) 10175–10180.
[27] D. Lin, H. Wu, R. Zhang, Chem. Mater. 21 (2009) 3479–3484.
[28] Z. Liu, D.D. Sun, P. Guo, Nano Lett. 7 (2007) 1081–1085.
[29] L. Narayanan, E. Bae, W. Choi, J. Phys. Chem. C 111 (2007) 15244–15250.